Article

Effective Height of a Floor Splitter Anti-Vortex Device under Varying Flow Conditions

Hyung-Jun Kim[1], Sung Won Park[2], and Dong Sop Rhee[3,*]

[1] Korea Institute of Construction Technology; john0705@kict.re.kr
[2] Korea Institute of Construction Technology; parksungwon@kict.re.kr
[3,*] Korea Institute of Construction Technology; dsrhee@kict.re.kr; Tel.: +82-31-910-0396

Abstract: A pump station is a very important flood control facility for mitigating inundation of urban lowland areas. It is not easy to secure a site to increase the capacity of a pump station in an urban area because of various limitations or to maximize the discharge capacity of the pump sump. Adding a facility to improve the pump capacity of a pump station may affect the flow characteristics, such as unexpected increases in the flow velocity and vorticity, and cause severe problems with operating the pump station. To solve those problems, anti-vortex devices (AVDs) have been developed and adopted for appropriate design standards. The Korean design criteria for AVDs are based on experience and foreign standards because not enough data on the AVD are available. In this study, the flow in the sump was numerically simulated at various AVD heights to collect information on improving the design and efficiency of a pump station. Consequently, an appropriate height for the AVD and changes in the flow pattern and vortex in the pump sump were determined and compared with 12 cases of inflow conditions with respect to the vertical location.

Keywords: Pump station, Sump, Anti-vortex device, Flow pattern, Vortex

1. Introduction

Urban floods due to unexpected severe rainstorms have become a serious problem in many countries. Furthermore, lowlands at urban riverfronts are very vulnerable to floods; most flood damage typically occurs in these areas. Thus, reliable and effective urban flood control facilities are needed to improve flood safety in lowlands. Various flood control facilities can be adopted as structural countermeasures to mitigate flood risk in urban lowlands. The pump station is a very efficient flood control facility that discharges the water inundating the lowland into the watershed.

A pump station is one of the most important flood control facilities for mitigating lowland flooding. Unexpected rainfall due to climate change increases the occurrence of abnormal floods that threaten people and their properties in flood-vulnerable areas. A pump station has to treat incoming flow over the design capacity to minimize flood damage. During pumping operation, a wide range of flood conditions can occur with variations in the river water level and changes in the sewage flow. This variation generates unsteadiness and instability of the sump pump, which decreases the pump capacity through cavitation, flow separation, pressure loss, and variation. In particular, air-entrained free-surface and subsurface vortices in pump sumps seriously damage the pump system. Various numerical and experimental studies have been performed on preventing the pump station capacity from being degraded by abnormal conditions in the sump pump.

For instance, Arboleda and El-Fadel [1] did a case study on sump design by using a hydraulic model and investigated the effect of several design features and site constraints on the hydraulic performance and sump configuration. Bauer and Nakato [2] studied the flow field formed in a pump sump by experimental observation. The operating conditions were changed to determine their effect on the formation of vortices around a bell mouth. Constantinu and Patel [3] applied a numerical k-$\boldsymbol{\varepsilon}$

turbulence model to capture the location, size, and strength of vortices. Their results showed that the numerical model can reproduce the flow pattern in a sump pump but should be validated with experimental observations. Rajendran et al. [4] installed a vertical suction pipe in a rectangular channel, measured the flow characteristics with a particle image velocimetry (PIV) experiment, and performed a numerical analysis. Rajendran and Patel [5] performed detailed measurements of vortices in the pump intake bay of a laboratory model comprising a vertical intake pipe with a bell mouth by PIV to improve the understanding of vortex formation in the bay. Their experiments demonstrated the usefulness of PIV in obtaining quantitative information on the number, location, and size of the vortices that is required to develop and validate numerical models of pump intake flows. Nagahara et al. [6] investigated the velocity distribution around submerged vortex cavitation in a pump intake in detail by using PIV. Choi [7] installed an experimental model of a suction cistern and used PIV to observe the flow characteristics in the sump. Nagahara et al. [6] conducted experimental and numerical analyses on the flow structure around a suction pipe due to an asymmetric flow velocity toward the water course direction in the suction cistern. The Turbomachinery Society of Japan (TSJ) [8] amended the standard for pump suction cisterns and reviewed the applicability of various numerical models for the same analysis target. Johansson et al. [9] conducted a model study on a sump through a physical test and computational fluid dynamics (CFD) and showed how hydraulic models are used to identify unacceptable flow conditions such as surface vortices, any high swirl, pre-rotation, and non-uniform axial velocity distribution at the bell mouth. They used the results to derive modifications for improving the hydraulic performance in both circulating water and cooling water pump intakes. Okamura et al. [10] conducted a hydraulic experiment similar to the benchmark test of TSJ and verified the accuracy of various numerical models. Park and Roh [11] reproduced the flow of the Japanese standard simple sump model of TSJ by using a CFD model and observed the generation of free surface and underwater vortices. Kim et al. [12] used the ANSYS-CFX model to analyze the effects of the gap between an underwater cargo pump inlet and sump on the suction performance. Choi et al. [13] simulated the flow homogeneity of pump stations with multiple sumps by using numerical analysis and analyzed the effects of the flow field depending on whether not an anti-vortex device (AVD) has been installed. Choi et al. [14] reproduced the benchmark experiment of the TSJ by using a numerical model and analyzed the effects of an AVD on the pump efficiency by considering additional AVDs.

Various numerical and experimental techniques have been conducted to reproduce the flow characteristics of the pump station sump and prevent vortices. However, the design of pump stations is still insufficient. These previous studies usually focused on steady flow conditions for the incoming and outgoing flows of the pump station. Thus, present design techniques for sump pumps are not appropriate for operation under varying flood conditions and need to be tested under unsteady flow conditions. In this study, a numerical model was applied to analyzing the flow characteristic changes under varying flow conditions and finding the effective height of the attached sump pump facility that mitigates abnormal flow.

2. Anti-Vortex Device in Sump Pump

Abnormal flows such as cavitation, vortices, and flow separation decrease the pumping capacity of a pump station. In particular, an air-entrained vortex, which starts from the flow surface and wall of a sump, can seriously damage the pump system. Thus, an additional facility is used to improve flow characteristics by suppressing vorticity in the pump sump; this is called an AVD. The Hydraulic Institute [15] suggested several AVDs of various shapes. However, the detailed specifications of the AVD have not been provided; thus, a numerical or experimental investigation needs to be performed to determine the optimal height of the AVD prior to the design of the pump sump.

This paper presents a numerical investigation on the effective shape of a floor splitter. A splitter attached to the floor under the bell mouth is a typical AVD for reducing the vortices and pre-swirls in the pump sump. Figure 1 shows the AVD that was adopted in this study. This AVD has a bottom splitter to improve the flow characteristics near the bell mouth and side wall corner fillets to reduce the side wall vortices and swirls. The slope of each splitter and fillet is 45°, and the length from the

Preprints (www.preprints.org) | NOT PEER-REVIEWED | Posted: 3 October 2016 doi: 10.20944/preprints201610.0001.v1

back wall is 110 m. The height of the AVD was modified based on the results of the numerical tests to find the effective height.

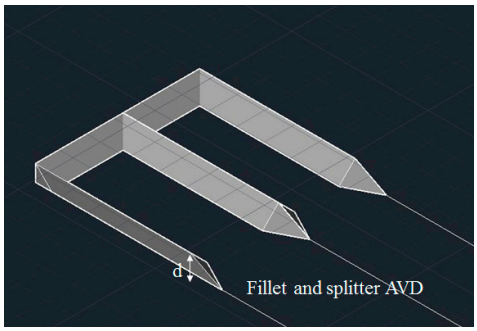

Figure 1. Anti-vortex devices for numerical cases

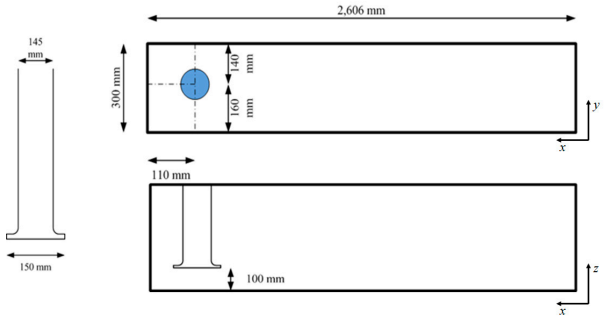

Figure 2. Schematic diagram of the experimental flume

3. Numerical Model

3.1. Mathematical Formulation

To reproduce the flow in the suction cistern, the three-dimensional model ANSYS-CFX was used. CFX is a three-dimensional flow analysis program developed by ANSYS that lets the user make both structural and non-structural tetrahedral grids for efficient grid formation. It also facilitates accurate flow analysis for the contact surface between a solid and liquid, such as the shear stress on the wall or bottom of the channel. It is governed by the continuity and momentum equations given below:

$$\frac{\partial \rho}{\partial t} + \nabla \cdot (\rho U) = 0 \tag{1}$$

$$\frac{\partial (\rho U)}{\partial t} + \nabla \cdot (\rho U \times U) = -\nabla p + \nabla \cdot \tau + S_M \tag{2}$$

$$\tau = \mu \left[\nabla U + (\nabla U)^T - \frac{2}{3} \delta \nabla \cdot U \right] \tag{3}$$

Here, ρ is the density of water (kg/m^3), U is the flow vector, p is the pressure, τ is a stress tensor related to the strain rate, and S_M is an external momentum generation term. A 3-D hexahedral-type grid was adopted for the flow simulation in the sump; the target area was idealized with a grid of approximately 1 million nodes; see Figure 2. To reproduce the flow, the boundary conditions of the pressure and outflow were applied at the inlet and outlet, respectively, and the shear stress transport (SST) model was applied as the turbulence model for calculating the conditions of the steady state. The SST model is an improved turbulence closure model that combines the advantages of the k–ε and

Preprints (www.preprints.org) | NOT PEER-REVIEWED | Posted: 3 October 2016 doi: 10.20944/preprints201610.0001.v1

k–ω models to achieve a wide range of applications. To achieve this purpose, the SST model adopts the blending function F1, which is equal to 1 near the solid surface and equal to 0 for the flow domain where wall friction is not dominant. It solves the k–ω equations in the near wall region and the k–ε equations for the rest of the flow. With this approach, the attractive near-wall performance of the k–ω model can be used without the potential errors resulting from the free stream sensitivity of that model. In addition, the SST model also features a modification to the definition of the eddy viscosity, which can be interpreted as a variable c_μ; in contrast, c_μ in the k–ε model is constant [16]. This modification is required to accurately capture the onset of separation under pressure gradients. In a recent NASA technical memorandum, the SST model was rated as the most accurate model in its class [17]. The SST model is similar to the standard k–ω model; its equations are given below:

$$\frac{\partial}{\partial t}(\rho k) + \frac{\partial}{\partial x_i}(\rho k u_i) = \frac{\partial}{\partial x_j}\left(\Gamma_k \frac{\partial k}{\partial x_j}\right) + G_k - Y_k \tag{4}$$

$$\frac{\partial}{\partial t}(\rho \omega) + \frac{\partial}{\partial x_i}(\rho \omega u_i) = \frac{\partial}{\partial x_j}\left(\Gamma_\omega \frac{\partial \omega}{\partial x_j}\right) + G_\omega - Y_\omega + D_\omega \tag{5}$$

Here, ρ is the density, k is the turbulent kinetic energy, and ω is the specific dissipation rate. G_k represents the generation of turbulent kinetic energy due to mean velocity gradients. G_ω represents the generation of ω. Γ_k and Γ_ω represent the effective diffusivities of k and ω, respectively. Y_k and Y_ω are the dissipations of k and ω due to turbulence. D_ω represents the cross-diffusion term.

3.2. Model Validation

The adopted model was applied to a benchmark test case for validation. Okamura et al. [10] experimentally investigated the generation of a stationary surface vortex, non-stationary surface vortex, and stationary subsurface vortex. The width of the channel was 300 mm, the suction pipe diameter was D = 145 mm, and the inlet was installed 100 mm from the bottom of the channel and 110 mm from the back wall. The center of the suction pipe was shifted 10 mm from the central line of the channel to produce a nonhomogeneous flow. The water level was 230 mm, and the output was 1.0 m^3/min (Fig. 1).

Figure 3 compares the 3-D numerical results of the present study and Okamura et al.'s experimental results using LS-PIV measurement [10] at the y-axis observation line crossing the center of the inlet on the x–y plane at z = 85 mm from the channel bottom. The x-directional flow velocity results showed better agreement with the observed flow velocity than the previous simulated results, and the results for the y and z flow velocities showed marked improvement over those of the previous study. The vorticity was considerably larger than the results of the previous numerical simulations and observed values on the right side of the channel, but it was mostly similar to the previous numerical simulations and observed values at the center or on the left. Based on this comparison, the numerical model implemented in this study was concluded to accurately reproduce the flow characteristics on the suction side.

4. Numerical Investigation

4.1. Test Cases and Computational Meshes

In order to determine the effective height of the splitter/fillet AVD, it was applied to the TSJ benchmark test, and additional various flow conditions were considered. These are described in Table 1. The adopted AVD heights were set according to the ratio with the bell mouth diameter in a range of 0.1–0.4. The flow depth range was 0.15–0.30 m with 0.05 m increments. Figure 1 describes the numerical mesh for the numerical simulation that was created by using the ANSYS Meshing tool. Figure 2 shows the pump sump model with an AVD installed. The inlet section at the entrance to the sump was set as the inlet boundary with hydraulic pressure according to the test case depth, and the mass flow was specified as an outlet section. Because of the huge burden of the 3D problem, the computation was distributed to 32 processors.

Preprints (www.preprints.org) | NOT PEER-REVIEWED | Posted: 3 October 2016 doi: 10.20944/preprints201610.0001.v1

Table 1. Locations of lines for results comparison

Items	Line 1	Line 2	Line 3	Line 4
Surface height z from the bottom of the channel (mm)	25	50	75	100
Line direction	y-axis crossing the center of the inlet			

4.2. Numerical Results

To analyze the appropriate installation height of the AVD at varying depth conditions, numerical simulations were conducted of 16 cases, which are presented in Table 2.

Table 2. Numerical test cases with various flow depths and AVD heights

Test case	AVD Height (h/D)	Flow Depth (m)
Case 1-1	0.1	0.15
Case 1-2		0.20
Case 1-3		0.25
Case 1-4		0.30
Case 2-1	0.2	0.15
Case 2-2		0.20
Case 2-3		0.25
Case 2-4		0.30
Case 3-1	0.3	0.15
Case 3-2		0.20
Case 3-3		0.25
Case 3-4		0.30
Case 4-1	0.4	0.15
Case 4-2		0.20
Case 4-3		0.25
Case 4-4		0.30

The changes in the flow velocity and vorticity along the x, y, and z axes were quantitatively compared, and Figure 3 presents the effectiveness of the AVD. Figure 4 shows the vortex zones created under different depth conditions in a waterway without the AVD. At the lowest inflow depth (H = 0.15 m), the vortex formed on the surface and at the wall influenced the induction pipe, which caused air entrainment. At greater inflow depths, the vortex zones decreased, and the flow became stabilized. Figure 5 shows the numerical simulation results for each depth of a waterway with an AVD installed. The AVD height was about 0.2 times the height of the induction pipe. Compared to the condition without the AVD, the vortex zones rapidly decreased even with the lowest inflow depth (H = 0.15 m). When the simulation result in which the depth gradually increased was compared with the result without the AVD in Figure 4, the vortex zone that started to emerge from the wall at H = 0.25 m was controlled. To quantitatively analyze the changes in the flow characteristics caused by the AVD, four sidetracks were set to compare the flow velocity and vorticity results. Table 1 presents the sidetracks.

Preprints (www.preprints.org) | NOT PEER-REVIEWED | Posted: 3 October 2016 doi: 10.20944/preprints201610.0001.v1

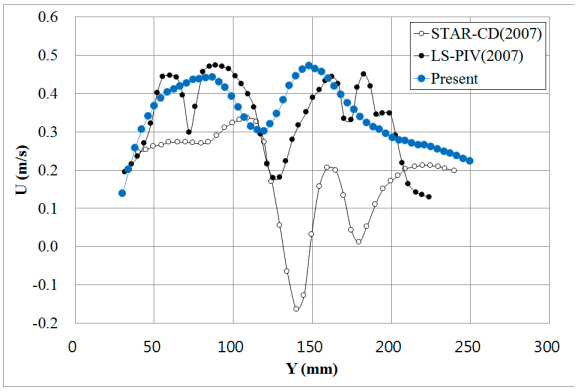

(a) x-directional velocity results

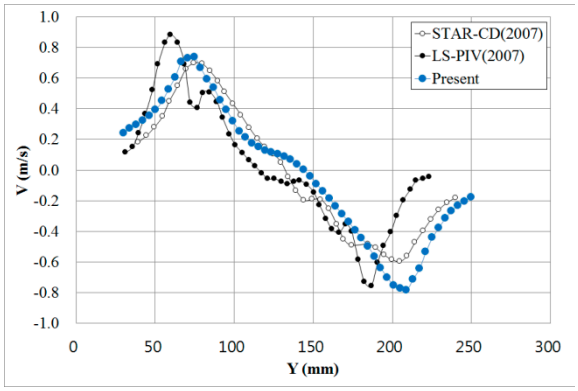

(b) y-directional velocity results

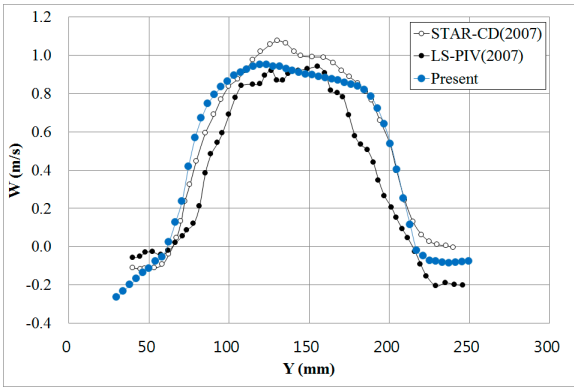

(c) z-directional velocity results

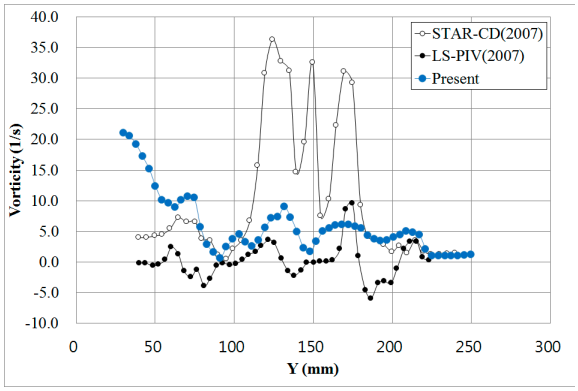

(d) Vorticity results

Figure 3. Comparison with previous research

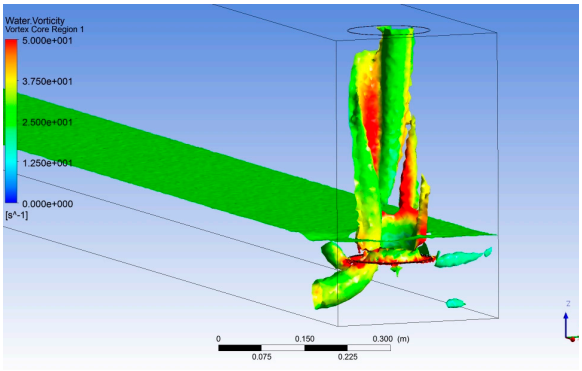

(a) Inflow depth H = 0.15 m

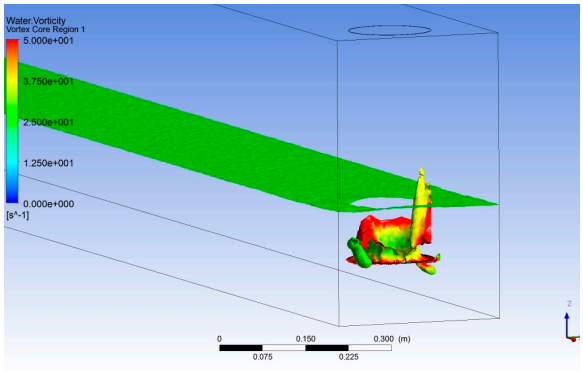

(b) Inflow depth H = 0.20 m

Preprints (www.preprints.org) | NOT PEER-REVIEWED | Posted: 3 October 2016 doi: 10.20944/preprints201610.0001.v1

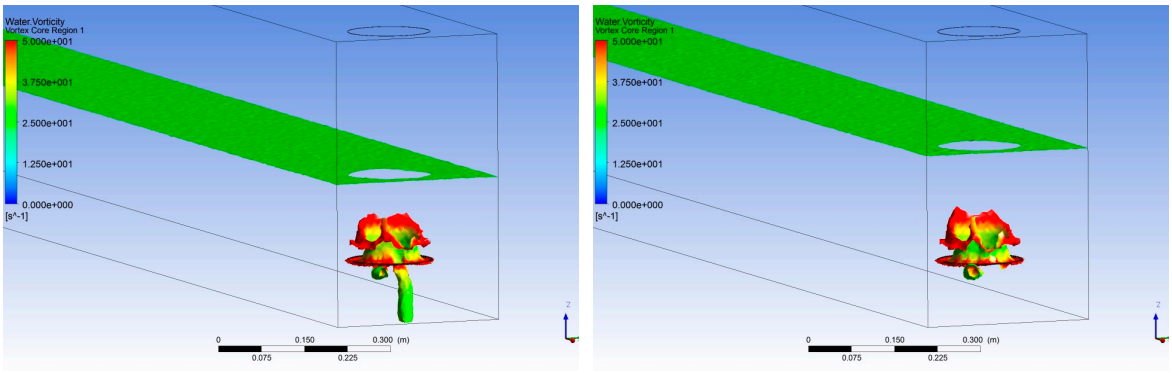

(c) Inflow depth H = 0.25 m (d) Inflow depth H = 0.30 m

Figure 4. Comparison of calculated vortex regions with changes in the inflow depth (without AVD)

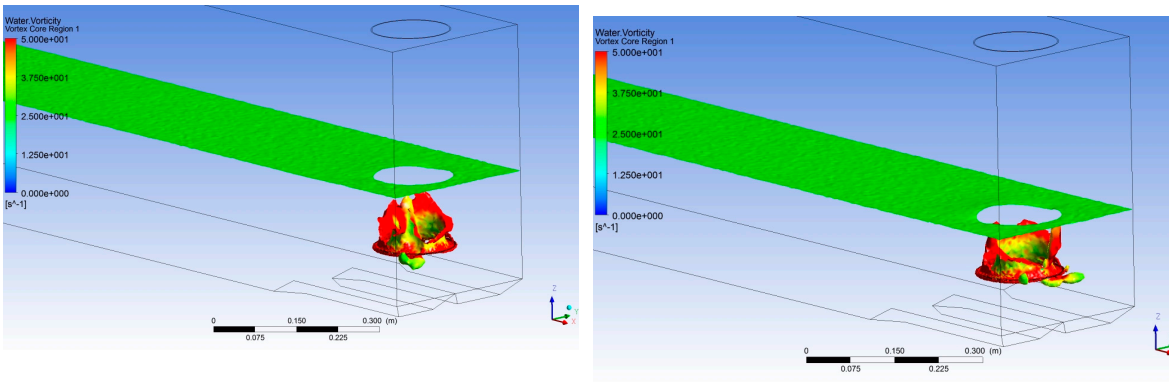

(a) Inflow depth H = 0.15 m (b) Inflow depth H = 0.20 m

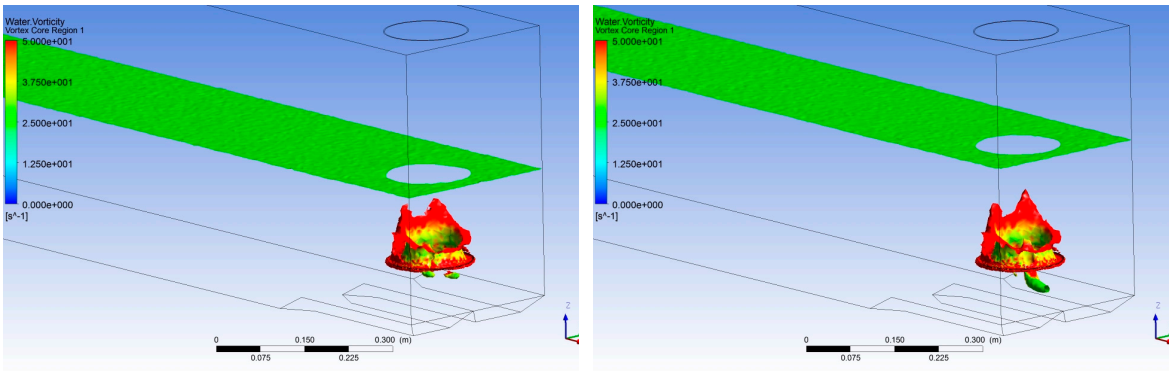

(c) Inflow depth H = 0.25 m (d) Inflow depth H = 0.30 m

Figure 5. Comparison of calculated vortex regions with changes in the inflow depth (AVD 0.2D)

Figure 6 shows the sidetrack results for the flow velocity along the x axis under varying depth conditions. Figure 6(a) shows the numerical simulation results at the lowest inflow depth of H = 0.15 m. Because of the presence of the AVD, the flow zone was reduced, so the overall flow velocity seemed to increase. However, when the AVD height was 0.2D, the flow velocity decreased. Figure 6(b) shows the numerical simulation results at the inflow depth of H = 0.20 m. In general, the flow velocity was reduced by the installed AVD. However, when the AVD height was 0.1D, the flow velocity around the induction pipe increased. Figure 6(c) compares the flow velocities along the x axis at the inflow depth of H = 0.25 m. When the AVD was present, the flow velocity increased. When the height was 0.2D, the flow velocity decreased at the area near the water depth. Figure 6(d) shows

Preprints (www.preprints.org) | NOT PEER-REVIEWED | Posted: 3 October 2016 doi: 10.20944/preprints201610.0001.v1

the numerical simulation results at the deepest inflow depth of H = 0.30 m. When the AVD was installed, the flow velocity along the x axis increased in general. However, when the installation height was 0.2D, the flow velocity was somewhat similar to that prior to the installation or reduced.

Figure 7 shows the changes in the flow velocity along the y axis when an AVD was installed according to the numerical simulation. Figure 7(a) shows the result at the low inflow depth of H = 0.15 m. Because of the reduced flow zone, the flow velocity increases. However, at the installation height of 0.2D, the flow velocity decreased. Figure 7(b) shows the result at the inflow depth of H = 0.20 m. Because of the AVD, the flow velocity changes along the y axis were not so significant. At the AVD height of 0.2D, the flow velocity was reduced compared with the case prior to the installation. Figure 7(c) shows the result at the inflow depth of H = 0.25 m. When the AVD height was 0.3D, the flow velocity increased at a zone close to the waterway floor. In other cases, the flow velocity increased near the bell mouth because of the AVD. Figure 7(d) shows the numerical simulation result at the inflow depth of H = 0.30 m.

Figure 8 shows the changes in the flow velocity along the z axis. Figure 8(a) shows the numerical simulation results at the inflow depth of H = 0.15 m. The flow velocity along the z axis was reduced because of the AVD. Figure 8(b) shows the numerical simulation result at the inflow depth of H = 0.20 m; the changes in the flow velocity were not so significant. Figure 8(c) shows the numerical simulation result obtained at H = 0.25 m. The flow velocity was slightly reduced by the AVD in general. However, at a height of 0.3D, the flow velocity increased. Figure 8(d) shows the numerical simulation result at the deepest inflow depth of H = 0.30 m. The flow velocity changes along the z axis due to the AVD were not so significant.

Figure 9 quantitatively compares the vorticities, which indicated the quantitative changes to the vortices generated by the AVD. Figure 9(a) shows the condition when the vortex zone was largest prior to the installation of the AVD because the depth was shallowest. In general, the vorticity decreased from the waterway floor to the induction pipe. However, at the AVD height at 0.1D, the vortex on line 3 (z = 0.075 m) was bigger than that prior to the installation. Figure 9(b) shows the numerical simulation result at the inflow depth condition of H = 0.20 m. When the heights of the AVD were 0.2D and 0.4D, the vorticity decreased. However, under the other two conditions, the vorticity increased. Figure 9(c) shows the numerical simulation result at the inflow depth of H = 0.25 m. When the AVD height was 0.3D, the vorticity increased, which had the expected effect of AVD improving the flow characteristics. Figure 9(d) shows the numerical simulation result at the inflow depth of H = 0.30 m. When the AVD height was 0.2D, the vorticity was similar to that prior to installation. However, in the other cases, the vorticity increased.

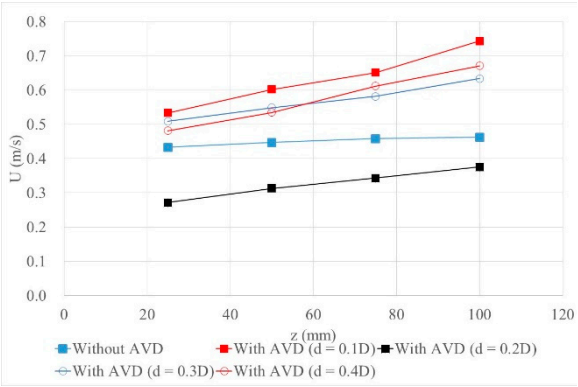

(a) Inflow depth H = 0.15 m

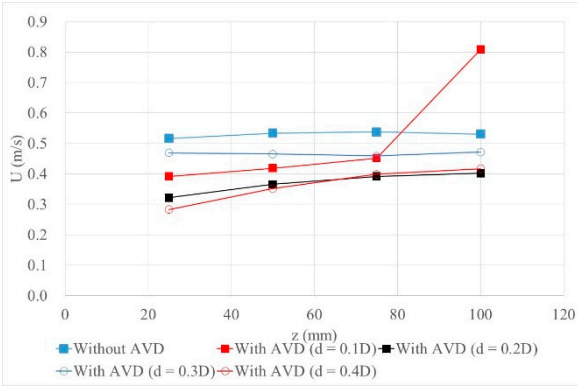

(b) Inflow depth H = 0.20 m

Preprints (www.preprints.org) | NOT PEER-REVIEWED | Posted: 3 October 2016 doi: 10.20944/preprints201610.0001.v1

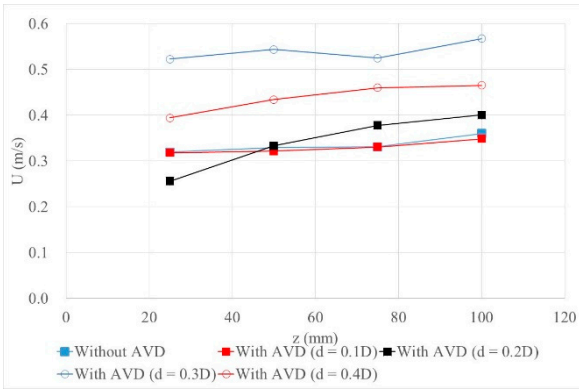

(c) Inflow depth H = 0.25 m

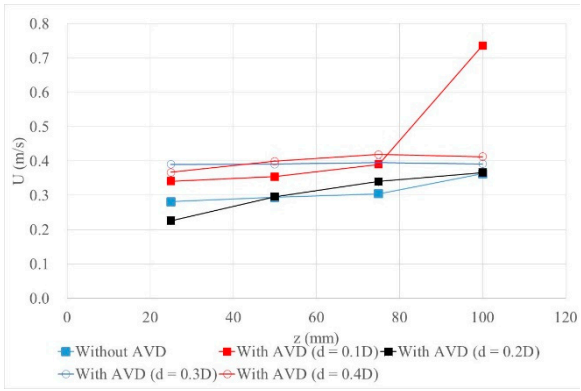

(d) Inflow depth H = 0.30 m

Figure 6. Comparison of calculated x-directional velocities with changing inflow depths and AVD heights

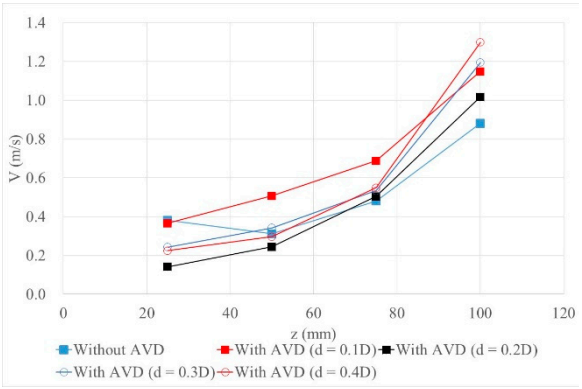

(a) Inflow depth H = 0.15 m

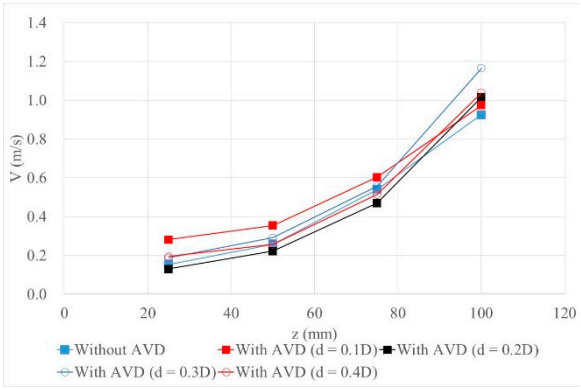

(b) Inflow depth H = 0.20 m

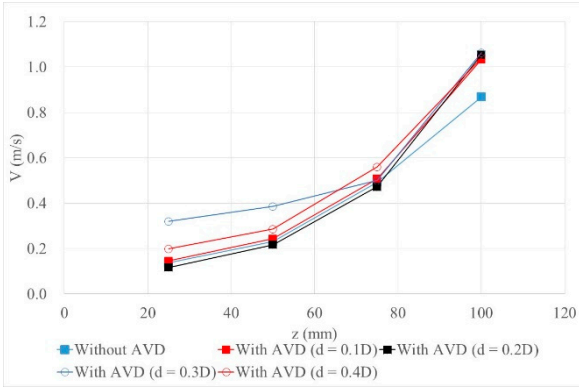

(c) Inflow depth H = 0.25 m

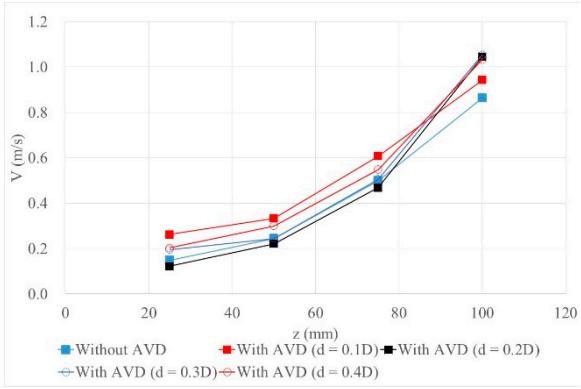

(d) Inflow depth H = 0.30 m

Figure 7. Comparisons of calculated y-directional velocities with changing inflow depths and AVD heights

Preprints (www.preprints.org) | NOT PEER-REVIEWED | Posted: 3 October 2016 doi: 10.20944/preprints201610.0001.v1

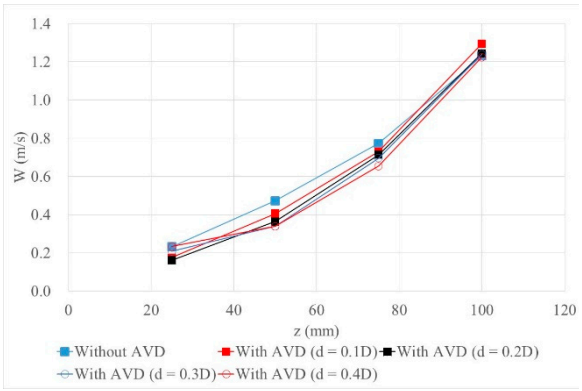

(a) Inflow depth H = 0.15 m

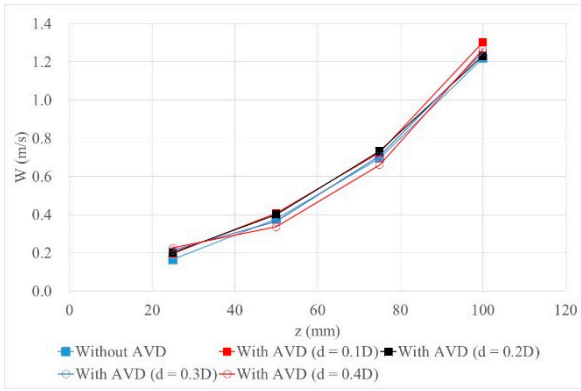

(b) Inflow depth H = 0.20 m

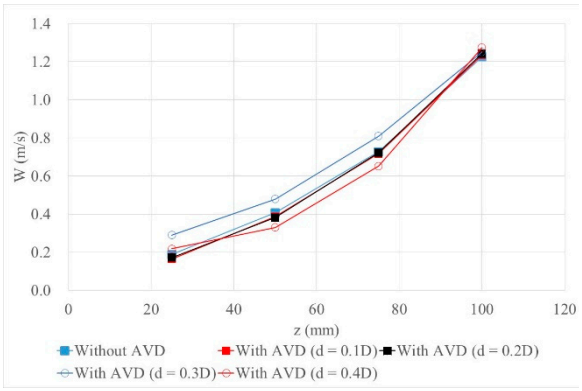

(c) Inflow depth H = 0.25 m

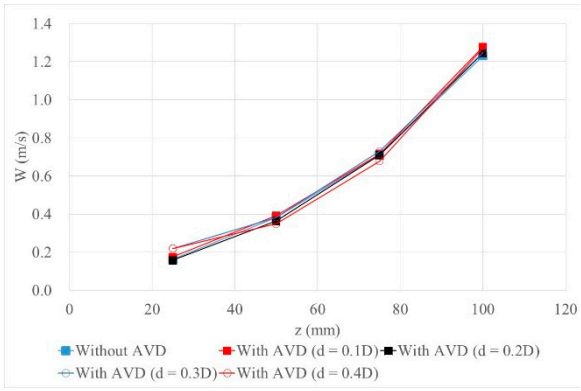

(d) Inflow depth H = 0.30 m

Figure 8. Comparison of calculated z-directional velocities with changing inflow depths and AVD heights

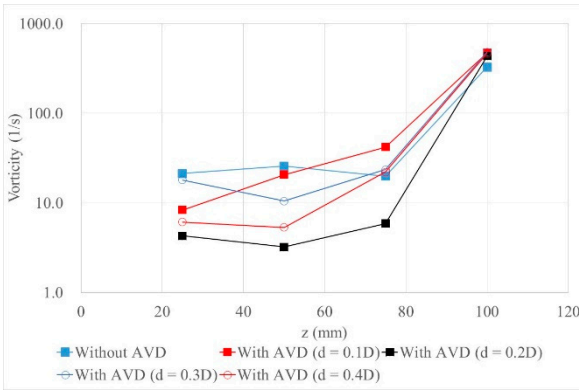

(a) Inflow depth H = 0.15 m

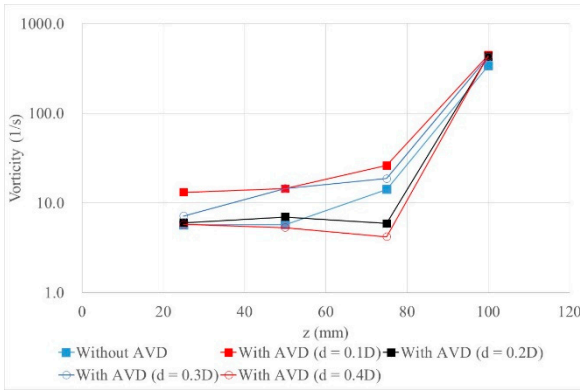

(b) Inflow depth H = 0.20 m

Preprints (www.preprints.org) | NOT PEER-REVIEWED | Posted: 3 October 2016 doi: 10.20944/preprints201610.0001.v1

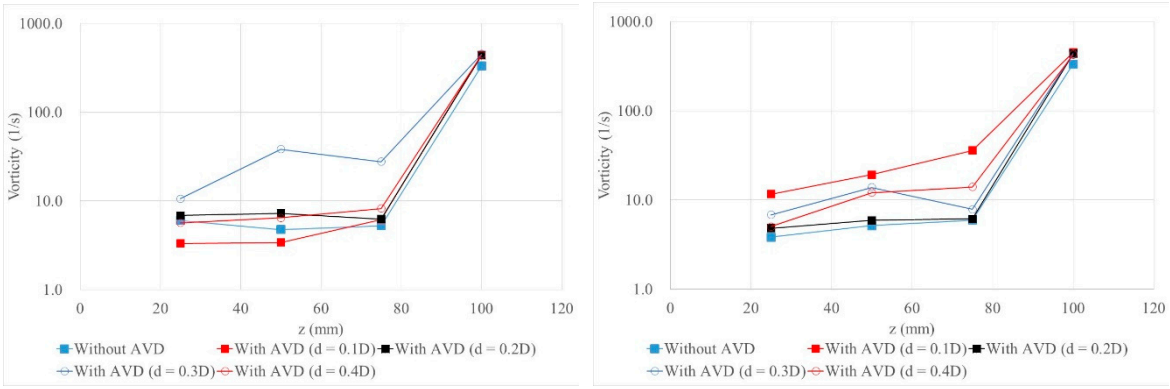

(c) Inflow depth H = 0.25 m

(d) Inflow depth H = 0.30 m

Figure 9. Comparison of calculated vorticities with changing inflow depths and AVD heights

5. Concluding Remarks

Flood pumping stations secure flood control of lowlands. Their design needs to reflect flow variations including hydrological characteristics. In the present study, numerical simulations were conducted to derive the AVD height for a suitable anti-vortex performance at various depth conditions, and the results were quantitatively compared. The results were as follows.

1. If flow stability is required because of a low inflow depth and high flow velocity, installing an AVD can reduce the flow velocity and vorticity of water induced through the induction pipe, which will improve the flow characteristics. However, the quantitative effects differ according to the height at which the AVD is installed. The height with the expected best effect is 0.2D, or about 0.2 times the diameter of the induction pipe.
2. Although the AVD is installed to improve the flow characteristics and prevent vortices under various depth conditions, improvement cannot be expected for all conditions. In some cases, the flow velocity and vorticity may even increase when an AVD is installed, which would worsen the flow conditions. Therefore, the appropriate installation height needs to be determined. If the flow conditions change, the installation height that should continue to provide improvement is 0.2D.

The above results can be utilized as a basis for designing flood pumping stations and can contribute to improving the performance of flood control facilities in response to climate change.

Acknowledgments: This study was funded by the Water Management Research Project of the Ministry of Land, Infrastructure, and Transport (13AWMP-B066744-01).

References

1. Arboleda, G.; El-Fadel, M. Effects of Approach Flow Conditions on Pump Sump Design. *J. Hydraul. Eng.* **1996**, *122*(9), 489–494. http://dx.doi.org/10.1061/(ASCE)0733-9429(1996)122:9(489)
2. Bauer, D. I.; Nakato, T. Subsurface Vortex Suppression in Water Intakes with Multiple-pump Sumps. IIHR Report No. 389, Iowa Institute of Hydraulic Research, University of Iowa, Iowa City, IA, **1997**.
3. Constantinu, G. S.; Patel, V. Numerical Model for Simulation of Pump-intake Flow and Vortices. *J. Hydraul. Eng.* **1997**, *124*(2), 123–134. http://dx.doi.org/10.1061/(ASCE)0733-9429(1998)124:2(123)
4. Rajendran V. P.; Constantinescu G. S.; Patel V. C. Experiments on Flow in a Model Water-pump Intake Sump to Validate a Numerical Model. *ASME FEDSM98-5098*, **1998**. http://dx.doi.org/10.1061/ (ASCE)0733-9429(1999)125:11(1119)
5. Rajendran, V.; Patel, V. Measurement of Vortices in Model Pump-Intake Bay by PIV. *J. Hydraul. Eng.* **2000**, *126*(5), 322–334. http://dx.doi.org/10.1061/(ASCE)0733-9429(2000)126:5(322)

6. Nagahara, T.; Sato, T.; Okamura, T. Measurement of the Flow around the Submerged Vortex Cavitation in a Pump Intake by Means of PIV. *Proceedings of the 5th International Symposium on Cavitation*, Osaka, Japan, November 1–5, **2003**, Cav03-OS-6-011.
7. Choi, J. W. A Study on the Flow Characteristics around Intakes within a Sump in a Pump Station by PIV. Master's Dissertation, Korea Maritime and Ocean University, Busan, Korea, **2003** (in Korean).
8. Turbomachinery Society of Japan. *Standard Method for Model Testing the Performance of a Pump Sump*, TSJ S002, **2005**.
9. Johansson, A. E.; Stacy, P. S.; White, D. K.; Lin, F. Advancements in Hydraulic Modeling of Cooling Water Intakes in Power Plants. *Proceedings of PWR2005*, Chicago, IL, **2005**; ASME Power, pp. 7–16, http://dx.doi.org/10.1115/PWR2005-50041.
10. Okamura, T.; Kamemoto, K.; Matsui, J. CFD Prediction and Model Experiment on Suction Vortices in Pump Sump. *Proceedings of the 9th Asian Conference on Fluid Machinery*, Jeju, Korea, October 16–19, **2007**, pp. 1–10.
11. Park, S. E.; Roh, H. W. CFD Prediction on Vortex in Sump Intake at Pump Station. *J. KSFM* **2007**, *10*(4), 39–46 (in Korean). http://dx.doi.org/10.5293/KFMA.2007.10.4.039
12. Kim, J. H.; Choi, Y. S.; Lee, K. Y. A Numerical Study on the Suction Performance of a Submerged Cargo Pump. *J. KSFM* **2008**, *11*(6), 18–23 (in Korean). http://dx.doi.org/10.5293/KFMA.2008.11.6.018
13. Choi, J. W.; Choi, Y. D.; Lim, W. S.; Lee, Y. H. Numerical Analysis on the Flow Uniformity in a Pump Sump Model with Multi-pump Intake. *J. KSFM* **2009**, *12*(4), 14–22 (in Korean). http://dx.doi.org/10.5293/KFMA.2009.12.4.014
14. Choi, J. W.; Park, N. S.; Kim, S, S.; Park, S. S.; and Lee, Y. H. Study on Performance Analysis of Pump within Sump Model with AVD installation by CFD. *J. KSWW*, **2012**, *26*(3), 463–469. http://dx.doi.org/10.11001/jksww.2012.26.3.463
15. Hydraulic Institute. *Pump Intake Design*, ANSI/HI, **1998**.
16. Carregal-Ferreira, J.; Holzwarth, A.; Menter, F.; Esch, T.; Luu, A. *Advanced CFD Analysis of Aerodynamics Using CFX*. AEA Technology GmbH: Otterfing, **2002;** pp. 1–14.
17. Bardina, J. E.; Huang, P. G.; Coakley, T. J. Turbulence Modeling Validation, Testing, and Development. NASA Technical Memorandum 110446, NASA, Washington DC, **1997**.